Hindawi
Advances in Civil Engineering
Volume 2022, Article ID 2296402, 15 pages
https://doi.org/10.1155/2022/2296402

Research Article

Analysis of the Influence of Whipstock Point Position of Directional Drilling through Embankment on the Stability of Embankment Slope against Sliding

Jinhuang Yu,[1,2] **Jinjie Liu**,[1,2] **Zhenzhen Jiang**,[1,2] **and Xiaofang Kang**[1,3]

[1]*College of Civil Engineering, Anhui Jianzhu University, Hefei 230601, China*
[2]*National Joint Engineering Laboratory for Building Health Monitoring and Disaster Prevention, Hefei 230601, China*
[3]*Key Laboratory of Intelligent Underground Detection Technology, Anhui Jianzhu University, Hefei 230601, China*

Correspondence should be addressed to Xiaofang Kang; xiaofangkang@ahjzu.edu.cn

Received 15 May 2022; Accepted 30 June 2022; Published 16 July 2022

Academic Editor: Tianshou Ma

With the increasing number of river-crossing pipeline projects, many studies have focused on the safety and stability of embankment slopes in horizontal directional drilling crossing embankment construction. In addition, it is challenging to study the influence of key processes in directional drilling construction on the antisliding stability of embankment slopes. A model of horizontal directional drilling crossing the Shaying River embankment was developed by using the numerical simulation software FLAC3D, and the strength reduction method is used to analyze the antisliding stability of the embankment after crossing the embankment. In this study, the effect of the position of the whipstock point on the antisliding stability of the embankment slope was considered. The analysis shows that when the inclined point is located below the center of the embankment, the anti-sliding stability of the embankment is the most unfavorable, and the construction should try to avoid the whipstock point below the center of the embankment. It was also determined that when the vertical distance between the oblique point and the crest of the embankment is exceeding 13 m, the impact on the antisliding stability of the embankment can be ignored.

1. Introduction

Horizontal directional drilling (HDD) pipe technology originated from the oil and natural gas industry [1]. It is a nonexcavation technology for laying underground pipelines [2]. It has the advantages of small environmental impact and no damage to structures. The construction process of this equipment has the advantages of no influence on the surrounding environment and long pipeline laying distance and can make the pipeline bypass the underground obstacles. Its construction is simple, fast, and economical. It has been widely used in gas and water pipeline laying projects in recent years. In this process, the drilling rig is first installed on the side of the Earth's entry point. Starting from the Earth entry point, along the designed line, a curve from the Earth entry point to the Earth entry point is drilled as the guiding curve of the preexpanding hole and the back-dragging pipeline [3, 4]. Then, different diameter diffusers are used to back-drag and expand the hole, and finally, the pipeline is back-dragged to the unearthed point. It plays a very important role in promoting the construction of underground pipelines in the world [5]. Article 1.4 of ASTM F1962-11 specifically states that this specification does not involve the application safety of horizontal directional drilling, and the application safety is the responsibility of users [6].

Now there are many theoretical studies on horizontal directional drilling; these studies mainly focus on mud pressure [7], HDD pull loads [8, 9], ground collapse [10], cuttings transport mechanism [11–13], and the alignment optimization of the pilot bore [14, 15]. Some people also used the finite element method to simulate the stability of the borehole [16, 17] and FLAC3D to simulate the land subsidence [18, 19]. Yin et al. [20] studied the safety impact of horizontal directional drilling through the embankment. In

the process of horizontal directional drilling crossing, there is a whipstock point in the transition part from the horizontal section to the arc section [21]. The whipstock point is the intersection of the horizontal section and the lifting section (the arc transition section) of the horizontal directional drilling [22]. The mechanical conditions at the whipstock point are very complex, which can easily cause some accidents. However, these studies did not consider the antisliding stability of the whipstock point position of the horizontal directional drilling on the embankment.

In this paper, firstly, the Swedish arc method, Bishop method, and Morgenstern–Price method are used to verify the strength reduction method to determine the feasibility of the strength reduction method and the accuracy of the parameters. By comparing and analyzing the safety factor and sliding surface diagram calculated by these methods, it can be concluded that the strength reduction method is feasible to analyze the stability of the embankment in the embankment project. After that, the safety and stability coefficients of embankment corresponding to different whipstock points in embankment engineering are comprehensively analyzed through the strength reduction program built-in FLAC3D finite-difference calculation software. Our findings can provide important technical guidance and support for flood control and disaster reduction in the water conservancy industry, construction of pipeline network crossing, and pipeline planning of other industries.

2. Engineering Overview and Calculation Parameters

The water distribution pipeline of a water plant in Jieshou City passes through the Shaying River once by horizontal directional drilling. The pipeline axis is orthogonal to the Shaying River. The minimum elevation of the channel crossing the pipeline is 23.30 m, the design elevation of the pipe top is 16.76 m, and the minimum distance between the pipe top and the river bottom is 6.54 m. The horizontal crossing section is mainly in the fourth layer of silty clay. The location and route of the borehole are shown in Figure 1. The layered description of engineering geological characteristics of foundation soil is listed in Table 1. According to the engineering geological survey report, the physical and mechanical indexes of each soil layer are listed in Table 2.

3. Numerical Modeling of the Embankment

3.1. Calculation Model Establishment. The left bank of Ying River crossing by directional drilling is selected as the calculation section, and the left side of the section is the backwater side and is the soil entry end of horizontal top line drilling. The right side of the section is the Shaying River waterward side. The cross section and soil layer distribution of the embankment is shown in Figure 2.

3.2. Determination of Model Boundary Conditions. In the calculation and analysis, it is necessary to ensure simulation accuracy and minimize the influence of the boundary effect. There are several basic assumptions in the calculation process. (1) The model does not consider the impact of time, only the impact of space. (2) The horizontal directional drilling crossing process is successful once without the influence of trajectory correction. (3) The model does not consider the effects of drill rotation and vibration on the stability of the embankment. (4) The influence of seepage on embankment safety is not considered.

During the construction of horizontal directional drilling, the slurry has the function of wall protection and lubrication, and the slurry pump will exert a certain pressure on the pipeline, so it is necessary to apply support pressure around the pipeline and the shaft wall, which is realized by applying normal stress on the interface between the pipeline and the soil. The supporting pressure around the shaft wall is calculated as follows:

$$\begin{aligned} P_b &= P_p - P_{dr} - P_{bn}, \\ P_{dr} &= \frac{f\rho Q^2}{\pi^2 R_1^5} L, \\ P_{bn} &= \frac{\rho}{2}\left(\frac{Q}{CA}\right)^2, \end{aligned} \tag{1}$$

where P_b is annular mud pressure, P_P is the real pump pressure, P_{dr} is the pressure loss, P_{bn} is the pressure loss through the drill nozzle, ρ is the density of drilling fluid, Q is volume flow, R_1 is the inner radius of the drill pipe, L is the length of drill pipe, f is friction coefficient, C is nozzle constant, and A is total nozzle area [23, 24].

In addition, the friction between the pipeline and the shaft wall should be considered in the dragging process of the pipeline, and a certain amount of friction will be generated on the contact surface between the two. However, the normal force conditions and the contact relationship between the pipeline and the shaft wall are complex in the friction generated in the dragging process of the pipeline. The force mechanism of the friction in this process also needs to consider the actual geological conditions and soil parameters. Therefore, the simulation calculation is simplified to simplify the calculation process of the numerical simulation. The specific simplifications are as follows. (1) Due to the drag force on the pipeline during the dragging process, the normal force point on the cross section of the pipeline is at the highest point of the cross section of the pipeline, and the other parts are not affected by the normal force; that is, on the cross section, only the highest point of the pipeline is affected by the friction force. (2) Divide the whole curve into i broken lines ($L_{b1}, L_{b2}, L_{b3} \ldots L_{bi}$). (3) Vertical loads on a pipe (including mud buoyancy, pipe weight, and pressure regulating pipe suspension) are simplified to net buoyancy. (4) Once the wall is formed, it has no significant influence on the equivalent stress and contact stress of the pipeline, so the wall and pipeline are considered rigid bodies [25]. The friction between pipe and

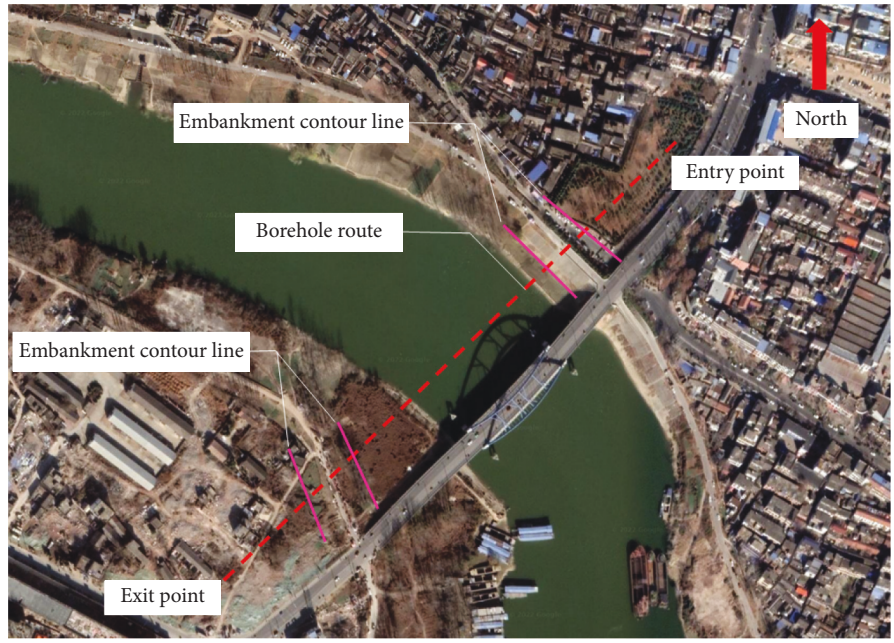

Figure 1: Location of the HDD river crossing (modified from Google Earth).

Table 1: Layered statistical table of geological characteristics of foundation soil.

Soil layer number	Name of soil layer	Feature description
1	Embankment filling (Q_4^{ml})	Gray-yellow, slightly wet, loose state, poor uniformity, mainly clay soil, containing a small number of plant rhizomes, local plain fill, medium-high compressibility
2	Silt with silty clay (Q_4^{ml})	Gray-yellow, very wet, loose-slightly dense state, local silt, low dry strength, low toughness, rapid shaking reaction, lusterless; silty clay, soft-plastic state, medium compressibility, medium-dry strength, medium toughness, no shaking reaction, slightly shiny
3	Clay (Q_3^{al})	Grayish yellow, plastic-hard plastic state, containing ferromanganese nodules and calcareous nodules, locally silty clay, medium compressibility, high dry strength, high toughness, no rocking reaction, and smooth section
4	Silty clay (Q_3^{al})	Gray-yellow, brown-yellow, plastic-hard plastic state, iron-manganese nodules and calcareous nodules, local clay, medium compressibility, medium-dry strength, medium toughness, no shaking reaction, slightly shiny

Table 2: Statistical table for calculating physical and mechanical parameters of rock and soil.

Soil layer number	Name of soil layer	Gravity γ/km·m^{-3}	Poisson ratio μ	Cohesion C/kPa	The angle of internal friction φ/(°)	Modulus of deformation/MPa
1	Embankment filling	19.1	0.30	15.0	13.1	26.1
2	Silt with silty clay	20.0	0.31	18.3	28	28.7
3	Clay	20.1	0.33	27.4	8.3	25.4
4	Silty clay	19.7	0.30	25.3	7.8	35.7

borehole wall is shown in Figure 3. The formula of friction is as follows:

$$f_{bi} = \int_i^{i+1} w_b g \mu_b \cos \beta_{bi} dL, \quad (2)$$

where f_{bi} is the friction force between the borehole wall and pipeline per unit length, i is broken line in the trajectory curve section of horizontal directional drilling, w_b is the net buoyancy per unit length of the pipe, μ_b is the coefficient of friction

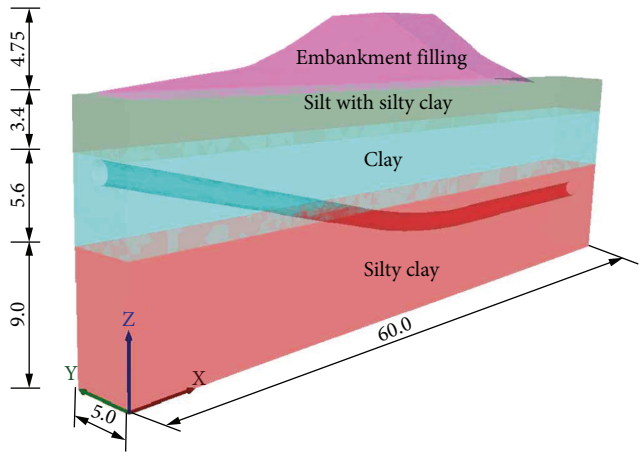

Figure 2: Chart of embankment section and soil layer distribution (unit: m).

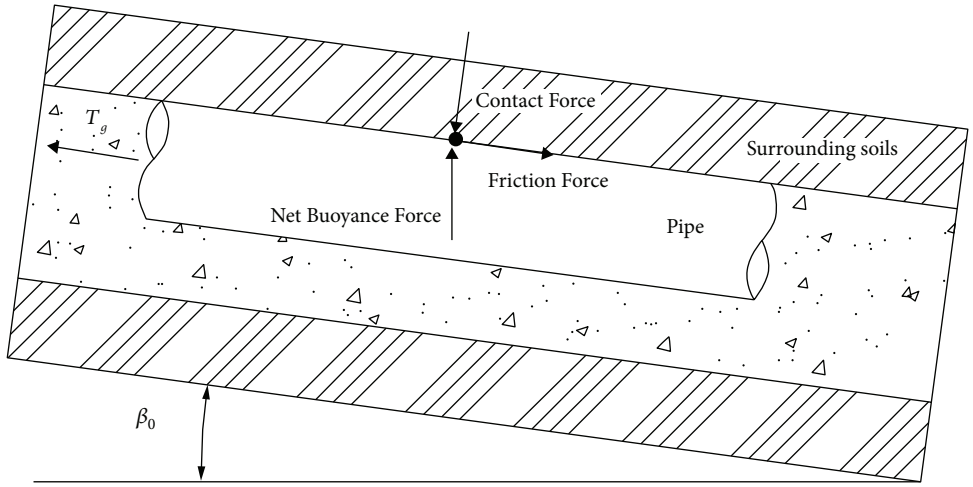

Figure 3: Diagram of friction between pipe and borehole wall.

between the pipe and the well wall, β_{bi} is the angle at which the pipe is tilted, and dL is the length of the unit pipe [26].

4. Methodology

The limit equilibrium method is a classical method in slope stability, which is recognized by most experts and scholars. It is often used in practical engineering and is generally accepted by the engineering community. In this section, the same calculation model is calculated and analyzed based on Auto Bank software and FLAC3D finite difference software. Swedish arc method, Bishop method, Morgenstern–Price method, and strength reduction method are adopted, respectively. The possible sliding surface and safety factor calculated by the four methods are compared to determine the rationality of model parameters and boundary conditions and the feasibility of the strength reduction method.

4.1. Validation. So far there is no analysis of the antisliding stability of horizontal directional drilling across the embankment. However, the accuracy of this study can be verified by the comparative analysis of the limit equilibrium method and the strength reduction method. Table 3 shows the safety factor of embankment antisliding stability and the comparison of relevant data. For the limit equilibrium method, the differences in FOS between this study and Burman et al. [27] and Kumar et al. [28] were only 2.7% and 1.1%, respectively. Moreover, For the strength reduction method, the difference in FOS between this study and Leshchinsky and Ambauen [29] and Memon [30] is 0.9% and 1.5%, respectively. The close comparison with previous work indicated that the accuracy of this study is reliable.

4.2. Stability Analysis of Embankment Slope by Limit Equilibrium Method

4.2.1. Swedish Arc Method. The Swedish arc method is the oldest and simplest method in the limit equilibrium method. In addition to assuming that the sliding surface is a cylindrical surface, it also assumes that the interaction force between soil strips is not considered, so there are some defects in theory. The safety factor is defined as the ratio of

Table 3: Summary of comparison with relevant published data.

	FOS	Difference (%)	References
Limit equilibrium method	1.237	2.7	Burman et al. [27]
	1.298	1.1	Kumar et al. [28]
	1.020	1.5	Leshchinsky and Ambauen [29]
	2.520	2.1	Memon [30]
Strength reduction method	1.310	4.1	Burman et al. [27]
	1.570	2.9	Kumar et al. [28]
	1.260	0.9	Leshchinsky and Ambauen [29]
	2.887	1.5	Memon [30]

the sum of antisliding torque provided by each soil strip on the sliding surface to the sum of sliding torque generated by external load and sliding soil on the sliding surface. The derivation formula of safety factor can be expressed as

$$F_s = \frac{\sum[c_i' l_i + (W_i \cos\alpha_i - \mu_i l_i)\tan\varphi_i']}{\sum W_i \sin\alpha_i}, \quad (3)$$

where F_s is the safety factor of soil slope stability against sliding, W_i is the weight of the soil itself, l_i is the length of the bottom of the soil bar, c_i' and φ_i' are the effective shear index of soil, α_i is the inclination of the bottom of the soil bar, and μ_i is the pore water pressure acting on the bottom of the soil strip [31]. Figure 4 is the schematic diagram of the possible sliding surface and the corresponding safety factor calculated by the Swedish arc method.

4.2.2. Bishop Method. Bishop method considers the interaction force between strips and blocks based on Swedish arc method, which can objectively reflect the force between strips and blocks. The calculation accuracy is sufficient, but it cannot be applied to any shape of the sliding surface. The derivation formula of the safety factor is as follows:

$$F_s = \frac{\sum_{i=1}^{n}(1/m_{\alpha i})[c_i b_i + (W_i - \mu_i b_i)\tan\varphi_i]}{\sum_{i=1}^{n} W_i \sin\alpha_i},$$
$$m_{\alpha i} = \cos\alpha_i + \frac{\tan\alpha_i \sin\alpha_i}{F_s}, \quad (4)$$

where F_s is the safety factor of soil slope stability against sliding, W_i is the weight of the soil itself, c_i' and φ_i' are the effective shear index of soil, α_i is the inclination of the bottom of the soil bar, μ_i is the pore water pressure acting on the bottom of the soil strip, and $m_{\alpha i}$ is the moment of horizontal additional force acting on the center of the sliding circle at the bottom edge of soil strip [32]. Figure 5 is the schematic diagram of the possible sliding surface and the corresponding safety factor calculated by the Bishop method.

4.2.3. Morgenstern–Price Method. The Morgenstern–Price method is a more general method, which is suitable for any shape of the sliding surface, but this strict calculation method has convergence problems [33]. Figure 6 shows the schematic diagram of the possible sliding surface and the corresponding safety factor calculated by the Morgenstern–Price method.

The safety factors calculated by the three methods are 3.47, 3.56, and 3.62, respectively. The Swedish arc method ignores the interaction force between strips and blocks, so the safety factor is lower than the other two methods. The safety factor calculated by the Bishop method and the Morgenstern–Price method is close. It can be seen from Figures 3–5 that, with the coordinate axis position as the origin, the center positions of the most dangerous sliding surface of the embankment calculated by the three methods are (26.43, 29.60), (36.09, 28.33), and (36.09, 26.63), respectively. The radii of the three most dangerous sliding surfaces are 14.89 m, 14.35 m, and 13.98 m, respectively, and the bottom of the sliding surface passes through the clay layer. Therefore, these three methods can be used to invert the model parameters, to determine the feasibility of the model parameters and the applicability of the strength reduction method.

4.3. Stability Analysis of Embankment Slope by Strength Reduction Method

4.3.1. Strength Reduction Method. FLAC (Fast Lagrangian Analysis of Continua) is a finite difference calculation software developed by ITASCA Company of the United States, also known as the Lagrangian element method program. FLAC3D is an extension program of FLAC, which not only includes all the functions of FLAC but also makes further development based on FLAC3D, so that it can simulate the stress and deformation of engineering structures in three-dimensional rock and soil and other media [34].

The strength reduction method is more rigorous than the limit equilibrium method in the theoretical system, which can fully meet the accuracy permission, strain compatibility, and the nonlinear stress-strain relationship of soil. Therefore, it is widely used in the stability analysis of various geotechnical engineering such as slopes.

The strength reduction method is used to calculate the slope stability in FLAC3D software. The principle is to gradually reduce the cohesion and internal friction angle of the model until the slope is destroyed. However, when the software executes the strength reduction program, it uses a kind of "bracket method," which means that the program first finds two "bracket" states of stability and instability of the model and then calculates by reducing the strength of the material to gradually reduce the tolerance between the two "brackets" until the tolerance between the stable solution and the unstable solution is less than the set value. Finally, the critical stability reduction factor F^{trial} of the slope is the

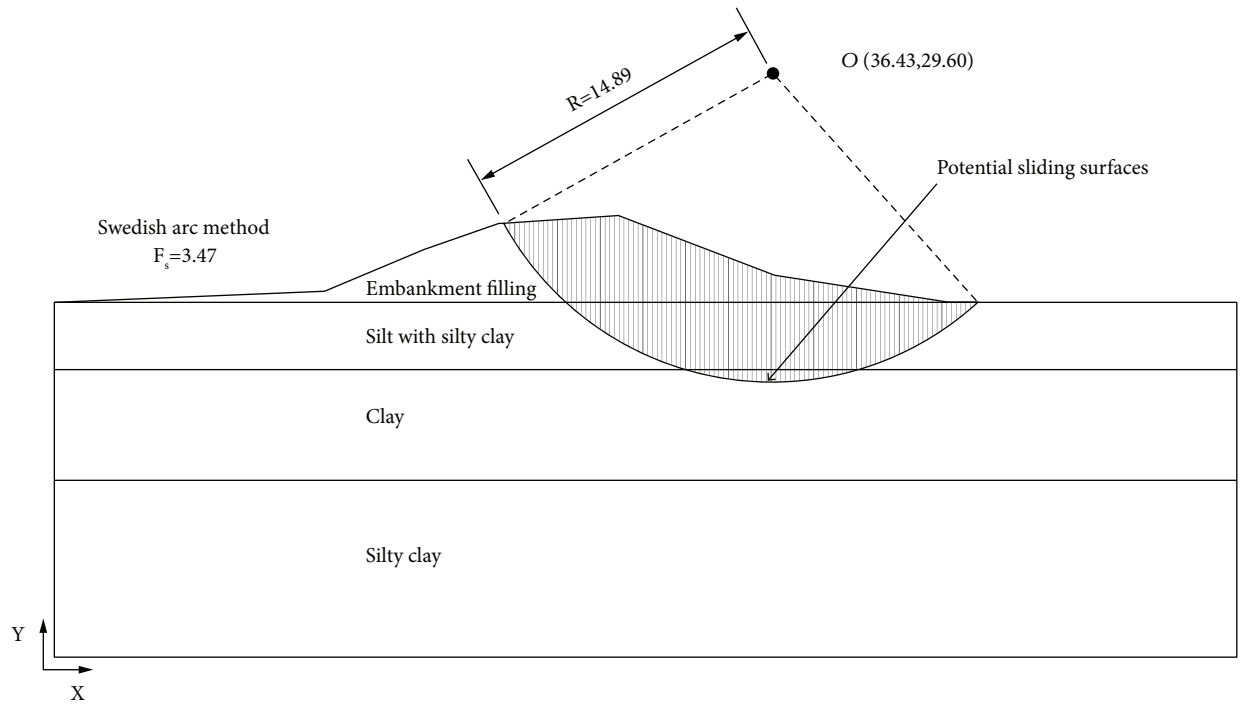

Figure 4: Schematic diagram of possible sliding surfaces calculated by Swedish arc method.

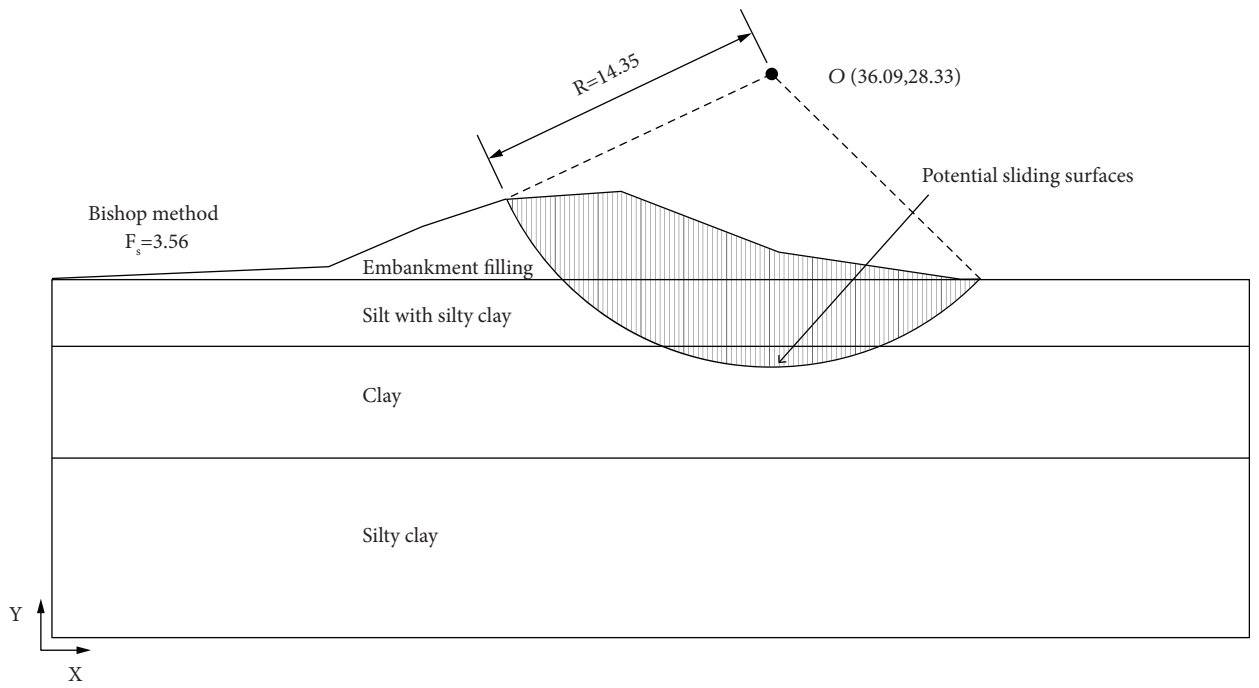

Figure 5: The schematic diagram of possible sliding surface calculated by the Bishop method.

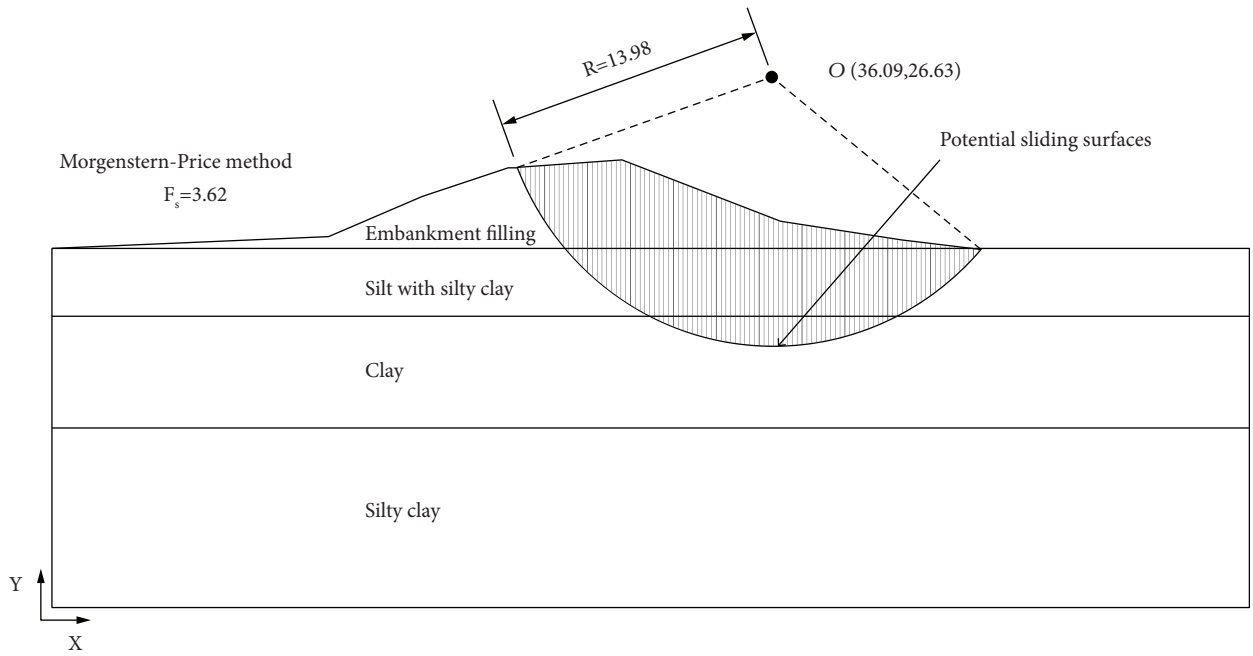

Figure 6: The schematic diagram of possible sliding surface calculated by the Morgenstern–Price method.

obtained safety factor [35]. The process of the strength reduction program is shown in Figure 7. The safety factor is defined as follows:

$$c^{trial} = \frac{c}{F^{trial}}, \qquad \varphi^{trial} = \arctan\left(\frac{\tan\varphi}{F^{trial}}\right) \tag{5}$$

c and φ are the Mohr–Coulomb parameters of undisturbed soil and c^{trial} and φ^{trial} are the Mohr–Coulomb parameters of the reduced soil.

4.3.2. Verification of Strength Reduction Method. Firstly, the Rhino software is used to establish the model, and the gridding of the model is carried out through the griddle. Then, the strength reduction program written by Fish language in the software is used for calculation. In addition, six displacement monitoring points are added in through the plastic zone to verify whether the displacement of points on this possible sliding surface conforms to the law. The calculated through plastic zone diagram is shown in Figure 8, the distribution of monitoring points is shown in Figure 9, and the displacement curve of monitoring points is shown in Figure 10.

It can be seen from Figures 7 and 8 that the most dangerous sliding surfaces calculated by the three limit equilibrium methods fall in the plastic penetration area calculated by the strength reduction method, and the safety factor calculated by the strength reduction method is 3.645, which is close to that calculated by the limit equilibrium method. The most dangerous sliding surface is found in the plastic penetration area. The radius of the circular sliding surface is 14.59 m, and the center coordinates of the circle are 35.98 and 28.57 (the position of the origin is the same as that of the origin arranged by the limit equilibrium method). Six displacement monitoring points are applied on the circular sliding surface. By observing the monitoring curves of these displacement points, the displacement variation in the Z direction is analyzed. It is found that the displacement variation of monitoring points 1 to 6 is consistent with the displacement variation of the sliding surface, which indicates that the parameters selected by the model are reasonable, and the strength reduction method is suitable for this calculation model.

5. Results and Discussion

In the process of horizontal directional drilling construction, there is a whipstock point in the middle of the construction from the horizontal stage to the upward stage. The mechanical situation near the whipstock point is particularly complex, which easily causes construction accidents. The horizontal and vertical distances between the whipstock point and the embankment will affect the antisliding stability of the embankment. The variation trend of the antisliding stability safety factor of the embankment is basically the same under the condition of different diameters changing in the position of the whipstock point. Therefore, the influence of whipstock point position change on the safety and stability of embankment under the condition of 1500 mm diameter is listed.

5.1. Influence of Horizontal Distance of Different Whipstock Points. The following conditions are analyzed: when the diameter of the pipe is 1500 mm, the angle of soil entry is 12°, and the horizontal pipe is 17.39 m away from the top of the embankment, the whipstock points are −9 m (position 1),

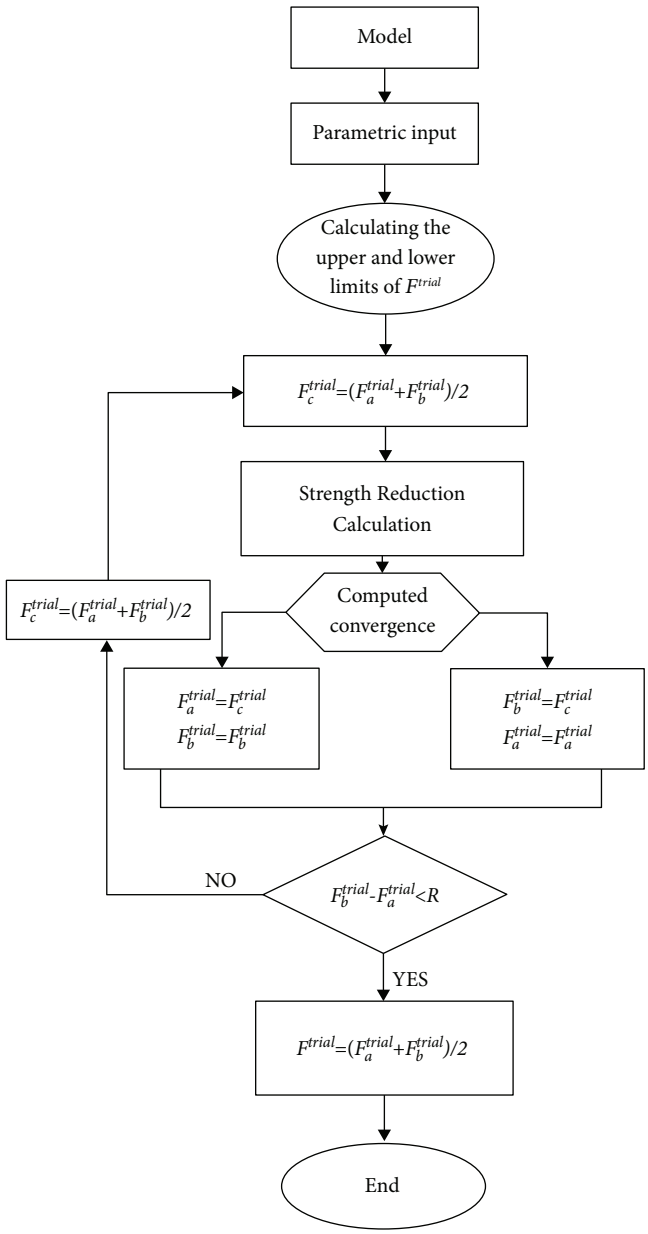

Figure 7: Flow chart of safety factor search program.

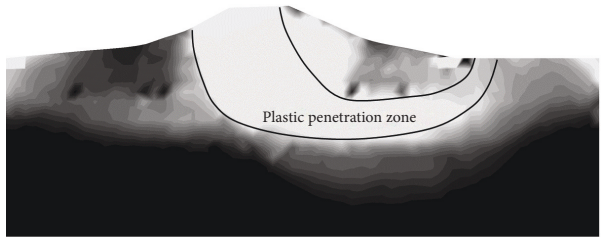

Figure 8: Schematic diagram of plastic penetration zone.

−6 m (position 2), −3 m (position 3), 0 m (position 4), 3 m (position 5), 6 m (position 6), and 9 m (position 7) away from the center of the top of the embankment, respectively, and the safety and stability of the horizontal directional drilling through the embankment are analyzed. The schematic diagram of the positions of different whipstock points is shown in Figure 11. The calculated safety factor is shown in Table 4, and the variation curve of the safety factor is shown in Figure 12. The corresponding displacement cloud is shown in Figure 13.

As can be seen from Figure 11, when the whipstock point of the horizontal directional drilling crossing trajectory is located in position 4, the overall stability of the embankment is the most unfavorable, and the safety factor decreases from 3.645 to 2.645, which is 27% lower than that without crossing the embankment. When the whipstock point changes from position 4 to position 1, the safety factor is generally on the rise, and the safety factor of the embankment is increased from 2.645 to 3.492. From the curve of safety factor and displacement contour, it can be seen that, under this condition, when the whipstock point of horizontal directional drilling trajectory is far away from the river and the center is greater than or equal to 9 m from the center of the crest, the influence of the whipstock point on the embankment can be basically ignored. When the whipstock point changes from position 4 to position 6, the stability of the slope facing the water surface is improved. When it is in position 7, the safety factor will be reduced. The reason is that the pipeline in the soil entry stage is too close to the vertical distance of the embankment, which affects the overall safety and stability of the embankment. The horizontal directional drilling angle should be reduced or the buried depth of the pipeline should be increased.

It can be seen from Figure 12 that when the whipstock point changes from position 1 to position 4, the point displacement of the potential sliding surface in the embankment increases and the sliding surface also has a downward trend. The radius of the sliding surface increases, and it tends to expand to the deep. When the whipstock point is located in position 4, the mud will exert radial stress on the surrounding soil, which will affect the overall stability of the embankment fill above. In addition, the extrusion of the pipeline and the soil will produce a downward additional thrust on the embankment soil, which also reduces the overall stability of the embankment. Therefore, it is necessary to strictly control the dragging speed and mud pressure during the construction process, so as to avoid cracks in the weak area of the embankment or mud flooding.

5.2. Influence of Different Vertical Distances of Whipstock Points. In this section, the diameter of the model is the same, the horizontal distance between the soil entry point and the embankment foot is the same, the horizontal distance between the whipstock point and the center of the embankment top is the same, and the buried depth of the horizontal section of the pipeline is different. The antisliding performance of the whipstock point on the embankment is analyzed by controlling the vertical distance between the whipstock point and the embankment top. A total of five groups of control tests were carried out, which were 17 m (position 1), 15 m (position 2), 13 m (position 3), 11 m (position 4), and 9 m (position 5) from the whipstock point

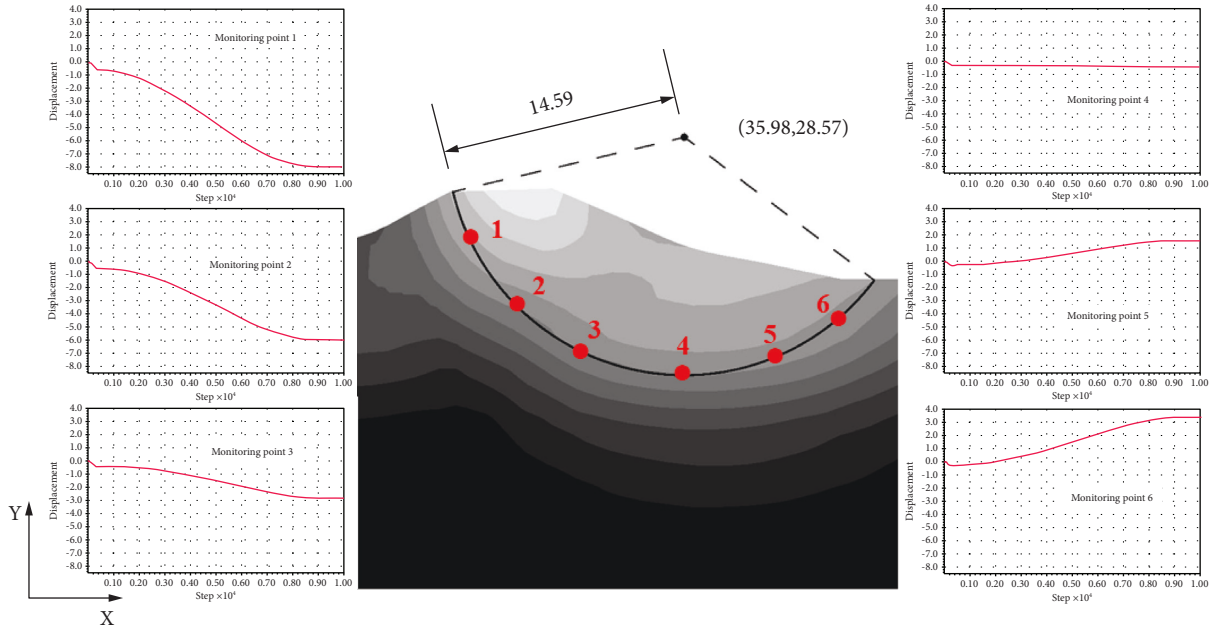

Figure 9: The distribution diagram of monitoring points.

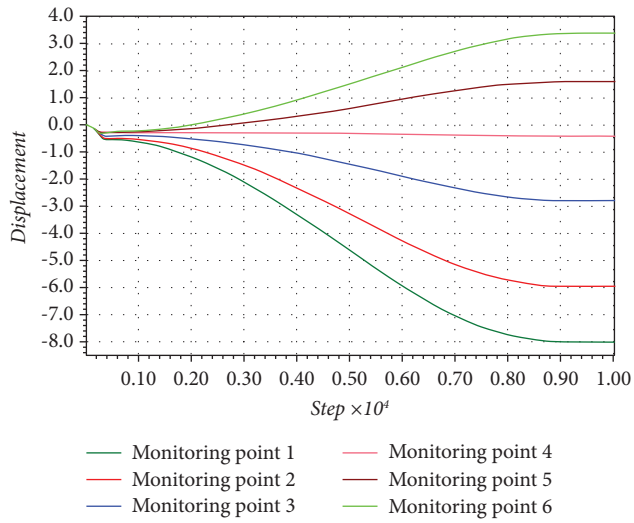

Figure 10: Diagram of displacement curve of monitoring points.

to the top of the embankment. The safety factor, displacement, and possible sliding surface of the five groups of models were observed to determine the optimal position of the whipstock point from the top of the embankment. The diagram of the vertical position distribution of different whipstock points is shown in Figure 14, the corresponding safety factor and change curve are shown in Table 5 and Figure 15, and the corresponding displacement cloud is shown in Figure 16.

It can be seen from Table 4 and Figure 14 that when the vertical distance between the whipstock point and the top of the embankment changes from 17 m to 9 m, the safety factor of the embankment slope decreases from 3.483 to 3.008, which is 14% lower than that of the condition with the distance of 17 m. When the vertical distance between the whipstock point and the crest of the embankment changes from 17 m to 13 m, the safety factor of the embankment slope decreases from 3.483 to 3.411, which is 2% lower than that of the

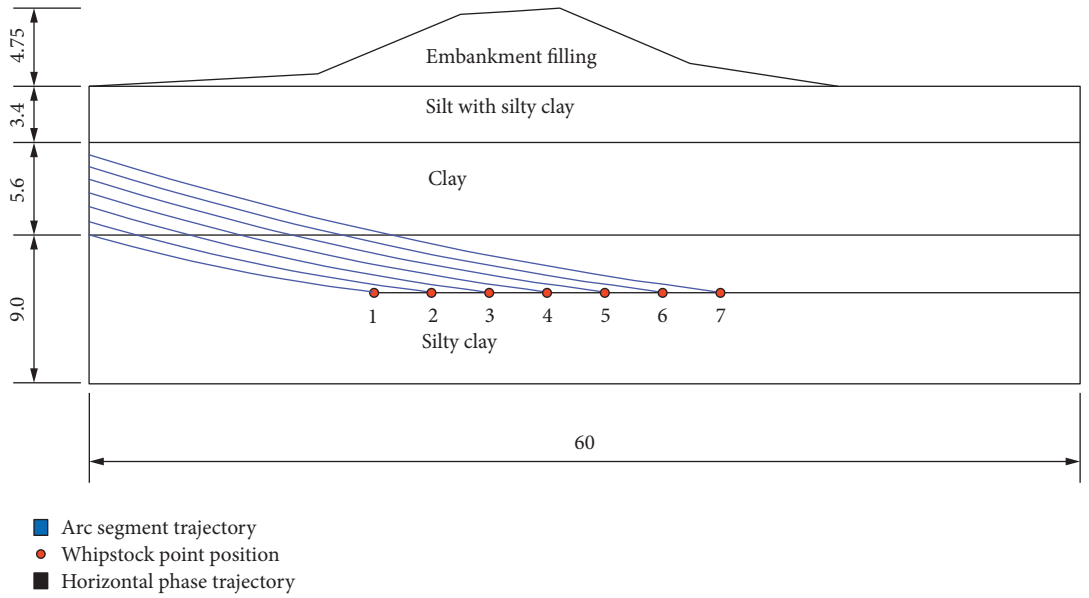

Figure 11: Indication diagram of different whipstock point positions (unit: m).

Table 4: Safety factors corresponding to different inclined positions.

Working condition	Distance from whipstock point to the center of the embankment (m)						
	−9	−6	−3	0	3	6	9
Factor of safety	3.492	3.117	3.245	2.645	3.023	3.305	2.711

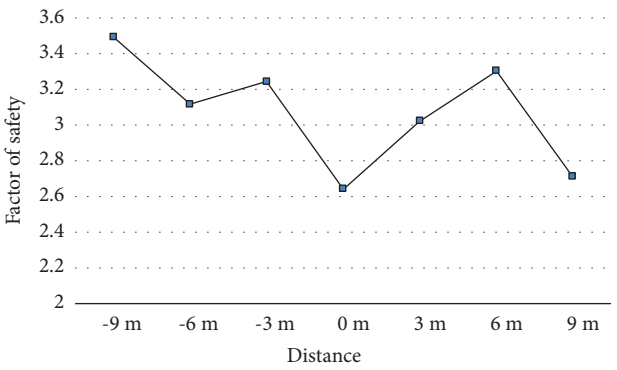

Figure 12: Variation curve of safety factor.

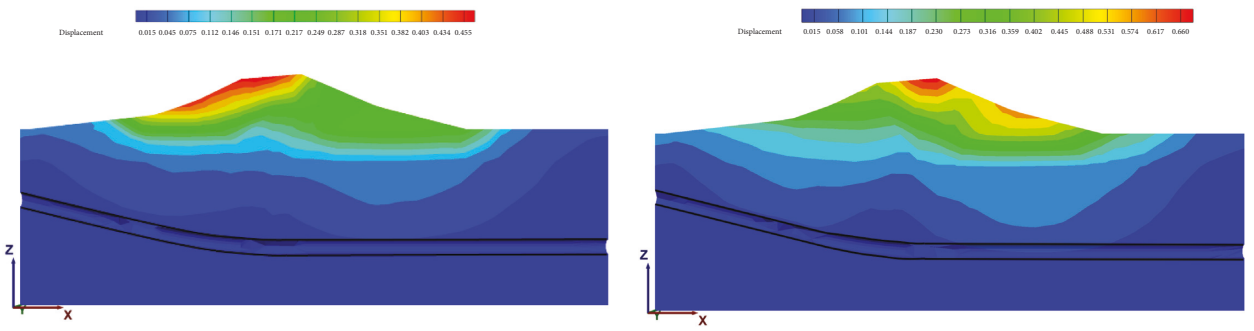

(a) (b)

Figure 13: Continued.

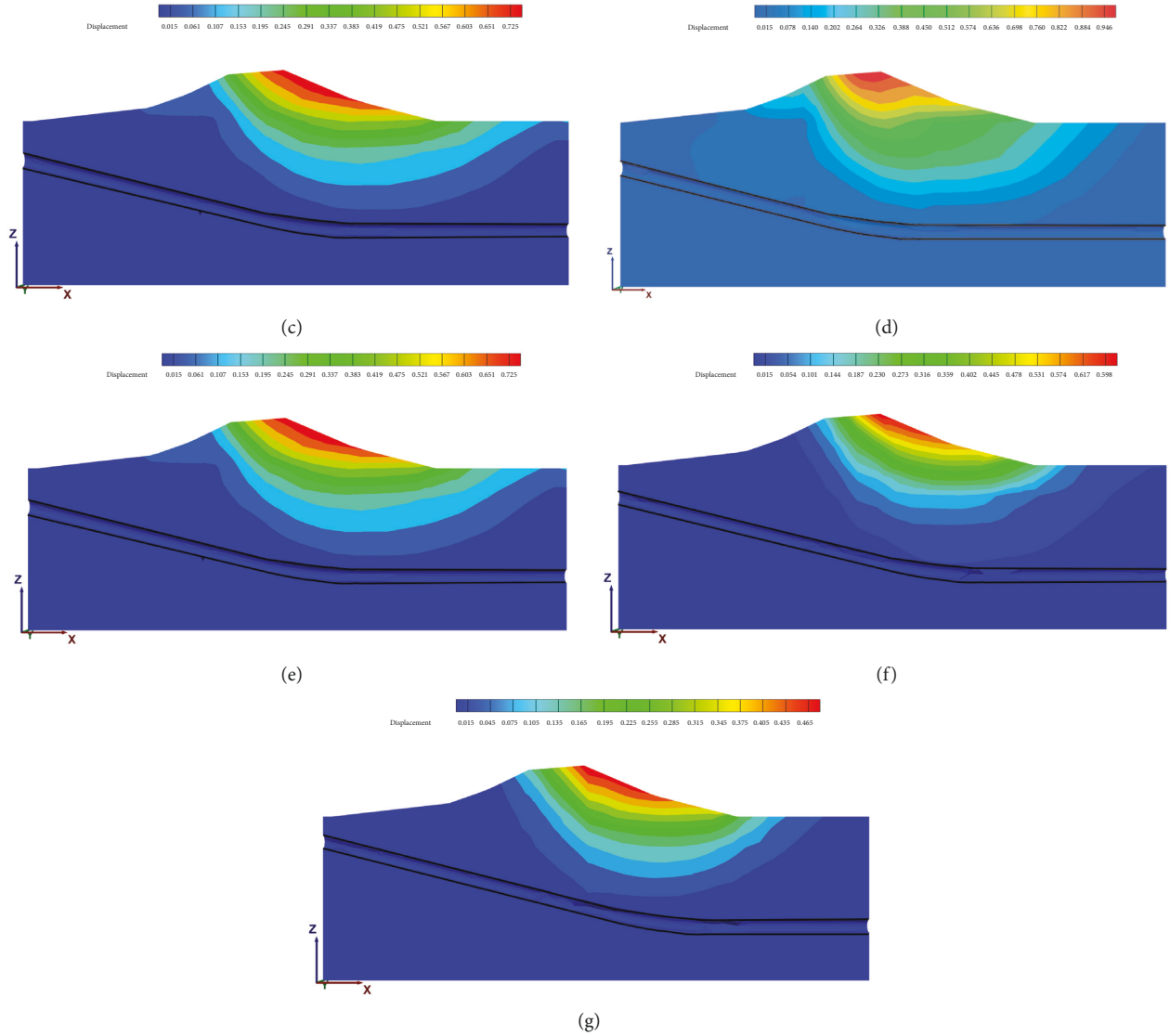

FIGURE 13: The contour of embankment displacement corresponding to different positions of whipstock points. (a) Position 1. (b) Position 2. (c) Position 3. (d) Position 4. (e) Position 5. (f) Position 6. (g) Position 7.

condition with the distance of 17 m. When the vertical distance between the whipstock point and the top of the embankment changes from 13 m to 9 m, the safety factor of the embankment slope decreases from 3.411 to 3.008, which is 12% lower than that of the working condition with the distance of 13 m. It can be seen that when the distance between the whipstock point and the top of the embankment is less than 13 m, the influence of the whipstock point on the embankment is more sensitive. From the displacement nephogram of Figure 15, it can be observed that when the whipstock point moves upward, the maximum displacement of the top of the embankment becomes larger, and the possible sliding of the embankment slope extends to the deep

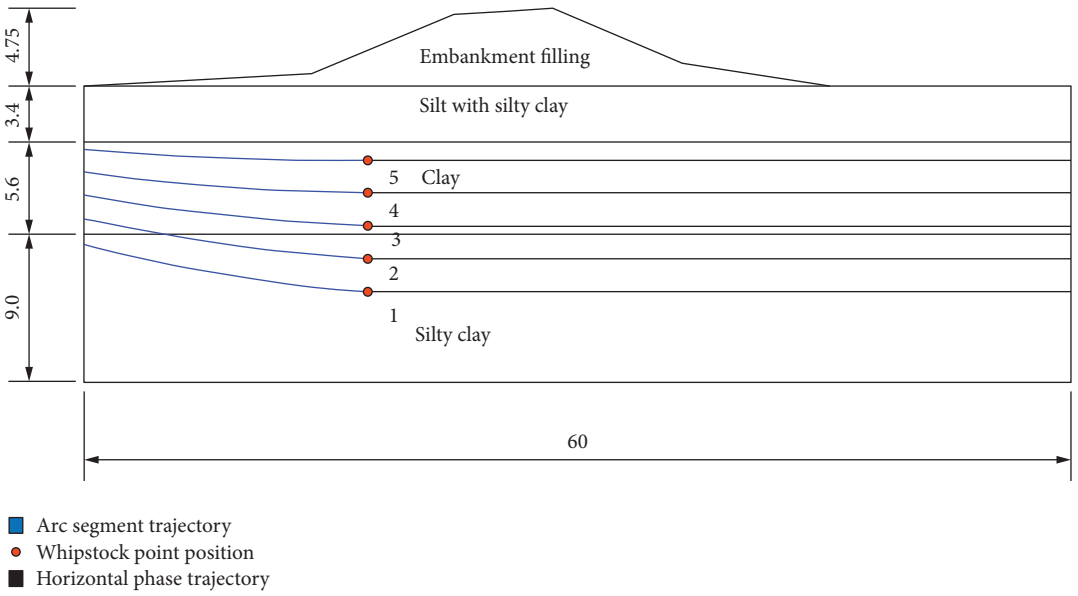

Figure 14: Schematic diagram of vertical positions of different whipstock points (unit: m).

Table 5: Safety factors corresponding to vertical positions of different whipstock points.

Working condition	Vertical distance from whipstock point to center of embankment (m)				
	17	15	13	11	9
Factor of safety	3.483	3.439	3.411	3.148	3.008

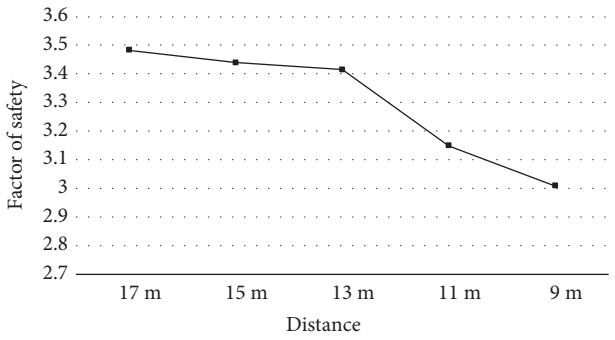

Figure 15: Variation curve of safety factor.

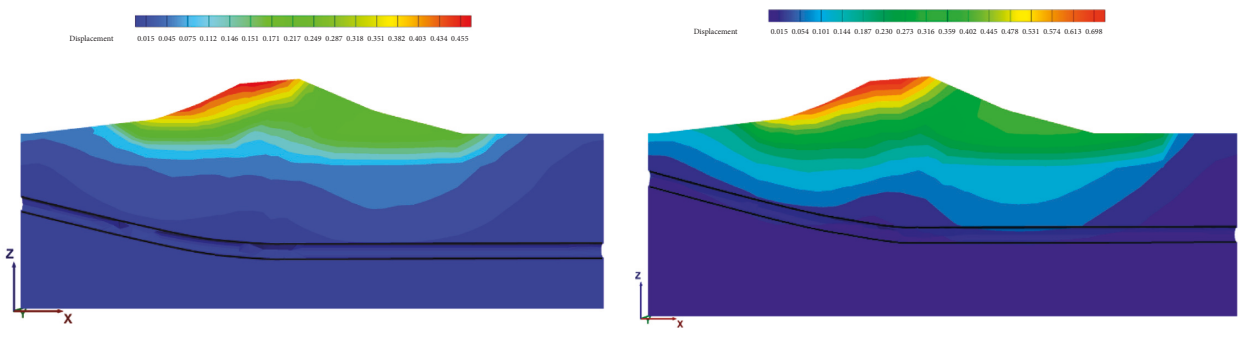

(a) (b)

Figure 16: Continued.

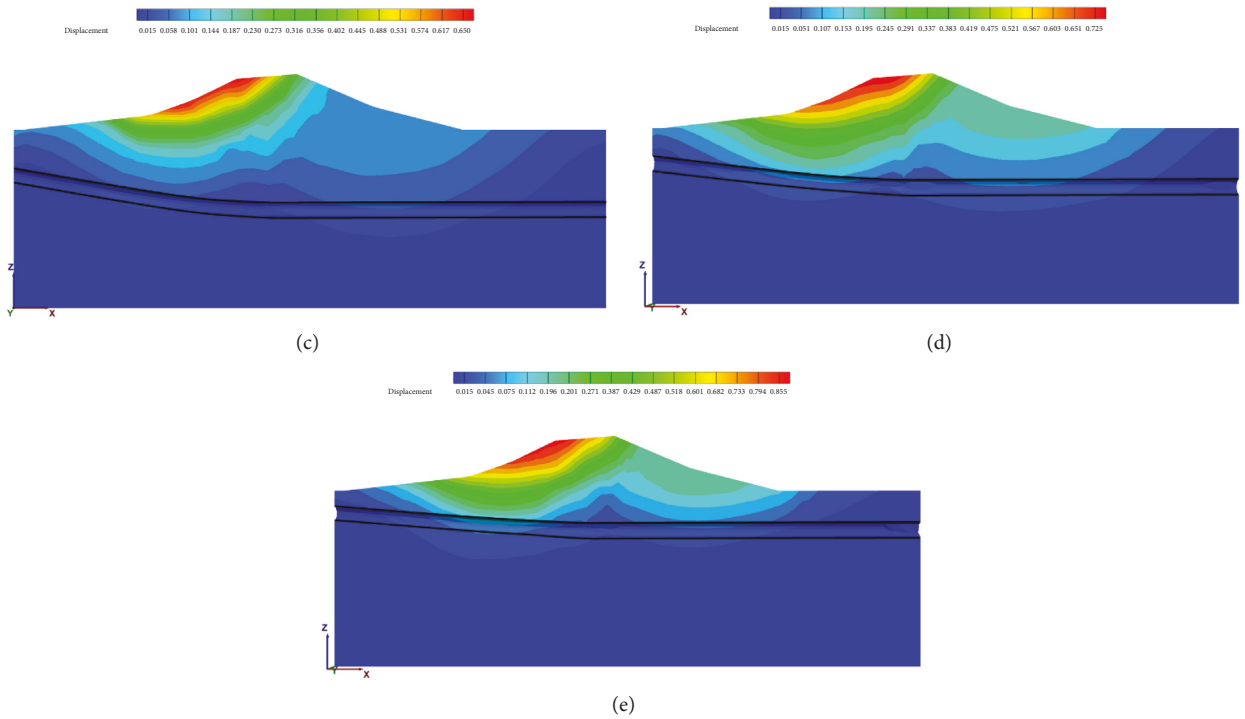

Figure 16: Embankment displacement nephograms corresponding to different vertical distances of building whipstock points. (a) Position 1. (b) Position 2. (c) Position 3. (d) Position 4. (e) Position 5.

layer, which also affects the stability of the borehole wall when the horizontal directional drilling passes through. Therefore, the vertical distance between the horizontal directional drilling crossing the dike whipstock point and the dike crest should be less than 13 m, and it is necessary to strengthen the monitoring of this area in order to control the parameters of horizontal directional drilling and minimize its impact on the dike.

6. Summary and Conclusions

(1) When FLAC3D was used to analyze the influence of horizontal directional drilling through the embankment, the selection and creation of the model, the consideration of boundary conditions, and the application of the initial stress field are very important. It is necessary to simulate the contact surface between the pipeline and the shaft wall in the actual construction process.

(2) In this paper, through the numerical simulation of the position of different whipstock points when the horizontal directional drilling crosses the embankment of Shaying River, it can be obtained that when the directional drilling crosses the embankment of Shaying River, the safety factor of the embankment stability was reduced by 27%; when the whipstock point was located below the center of the dike crest, it was the most unfavorable to the safety and stability of the dike. In construction, the whipstock point should be avoided from being located below the center of the dike crest.

(3) When the whipstock point of the horizontal directional drilling was far away from the river and the center was greater than or equal to 9 m from the center of the top of the embankment of Shaying River, the influence of the whipstock point on the embankment can be basically ignored. The vertical distance between the whipstock point of horizontal directional drilling and the top of the embankment should be greater than 13 m to minimize its impact on the embankment.

(4) Since there are many factors affecting the horizontal directional drilling through the embankment construction process and after the construction, and each factor is also interrelated, the research in this paper is also very limited and imperfect, and many problems need to be further studied and explored, such as the boundary conditions on the contact surface of the pipeline and the surrounding soil at the whipstock point and the influence of back-drag bit vibration; further research and discussion are needed on the side friction between pipeline and borehole wall in the process of towing. In addition, in the establishment of the model of directional drilling crossing the embankment, it is necessary to make general assumptions and finite assumptions on the model.

Data Availability

The data used to support the findings of this study are included within the article.

Conflicts of Interest

The authors declare that they have no conflicts of interest.

Acknowledgments

This study was supported by the Anhui Provincial Natural Science Foundation (Grant no. 2008085QE245), the Natural Science Research Project of Higher Education Institutions in Anhui Province (Grant no. KJ2019A0747), the School-Enterprise cooperative development project of Anhui Jianzhu University (Grant no. HYB20210178), the Project of Science and Technology Plan of Department of Housing and Urban-Rural Development of Anhui Province (Grant no. 2021-YF22), and the school-level scientific research project of Anhui Jianzhu University (Grant no. JZ202209).

References

[1] S. Abdollahipour, D. H. S. Jeong, R. R. Burman, and F. Gunsaulis, "Performance assessment of on-grade horizontal directional drilling," *Journal of Construction Engineering and Management*, vol. 138, no. 3, pp. 458–468, 2012.

[2] X. Yan, S. T. Ariaratnam, S. Dong, and C. Zeng, "Horizontal directional drilling: state-of-the-art review of theory and applications," *Tunnelling and Underground Space Technology*, vol. 72, pp. 162–173, 2018.

[3] J. Daniel, C. Penn, J. Antonangelo, and H. Zhang, "Physicochemical characterization of horizontal directional drilling residuals," *Sustainability*, vol. 12, no. 18, p. 7707, 2020.

[4] X. H. Zhu and Q. J. Yi, "Research and application of reaming subsidence control in horizontal directional drilling," *Tunnelling and Underground Space Technology*, vol. 75, pp. 1–10, 2018.

[5] J. Daniel, C. Penn, J. Antonangelo, and H. Zhang, "Land application of urban horizontal directional drilling residuals to established grass and bare soils," *Sustainability*, vol. 12, no. 24, p. 10264, 2020.

[6] F. Astm, *Standard Guide for Use of Maxi-Horizontal Directional Drilling for Placement of Polyethylene Pipe or Conduit under Obstacles, Including River Crossings*American Society for Testing Materials, West Conshohocken, PA, USA, 1962.

[7] X. F. Yan, H. T. Lan, I. D. Moore, and B. Ma, "Flow properties of fresh mud (drilling fluid) used in horizontal directional drilling," *Journal of Pipeline Systems Engineering and Practice*, vol. 12, no. 1, 2021.

[8] Z. W. Guo and Z. Liang, "Analysis of the pipeline pull-back load for horizontal directional drilling," *KSCE Journal of Civil Engineering*, vol. 22, no. 12, pp. 5133–5142, 2018.

[9] G. L. Xu, L. X. Cai, R. Ji, and Z. Wang, "Numerical simulation of pipe-soil interaction during pulling back phase in horizontal directional drilling installations," *Tunnelling and Underground Space Technology*, vol. 76, pp. 194–201, 2018.

[10] B. Shu and B. S. Ma, "Study of ground collapse induced by large-diameter horizontal directional drilling in a sand layer using numerical modeling," *Canadian Geotechnical Journal*, vol. 52, no. 10, pp. 1562–1574, 2015.

[11] B. Shu, B. S. Ma, and H. T. Lan, "Cuttings transport mechanism in a large-diameter HDD borehole," *Journal of Pipeline Systems Engineering and Practice*, vol. 6, no. 4, 2015.

[12] B. A. Shu and S. H. Zhang, "Cuttings transport in maxi HDD boreholes with front reaming and one way drilling mud return technologies," *Tunnelling and Underground Space Technology*, vol. 72, pp. 1–8, 2018.

[13] C. Zeng, X. F. Yan, Z. Zeng, and S. Yang, "The formation and broken of cuttings bed during reaming process in horizontal directional drilling," *Tunnelling and Underground Space Technology*, vol. 76, pp. 21–29, 2018.

[14] F. Patino-Ramirez, C. Layhee, and C. Arson, "Horizontal directional drilling (HDD) alignment optimization using ant colony optimization," *Tunnelling and Underground Space Technology*, vol. 103, Article ID 103450, 2020.

[15] P. Tervydis and R. Jankuniene, "Horizontal directional drilling pilot bore simulation," *Turkish Journal of Electrical Engineering and Computer Sciences*, vol. 25, no. 4, pp. 3421–3434, 2017.

[16] X. Wang and R. Sterling, "Stability analysis of a borehole wall during horizontal directional drilling," *Tunnelling and Underground Space Technology*, vol. 22, no. 5-6, pp. 620–632, 2007.

[17] P. Zhou, R. Jiao, B. Ma et al., "Analysis of borehole wall stability in horizontal directional drilling," in *Proceedings of the ICPTT 2012: Better Pipeline Infrastructure for a Better Life*, pp. 1816–1825, Wuhan, China, November 2013.

[18] P. Sun, C. An, and H. Cao, "Horizontal borehole displacement analysis based on drilling fluid pressure," *Chinese Journal of Underground Space and Engineering*, vol. 7, no. 6, pp. 1168–1173, 2011.

[19] P. Sun, H. Cao, L. Zuo, and Z. Wang, "Ground surface movement simulation due to HDD based on soil parameters," in *Proceedings of the ICPTT 2012: Better Pipeline Infrastructure for a Better Life*, pp. 1977–1988, Wuhan, China, November 2013.

[20] X. Yin, W. Lv, L. Xie, and S. Li, "Study on the pipeline crossing methods and suitability of engineering geological conditions in the middle reaches of the yangtze river," in *Proceedings of the ICPTT 2009: Advances and Experiences with Pipelines and Trenchless Technology for Water, Sewer, Gas, and Oil Applications*, pp. 1047–1055, Shanghai, China, September 2009.

[21] G. Mackenzie and S. B. Wilson, "Coiled tubing deployed reentry whipstocks-technology overview and case histories," in *Proceedings of the International Oil Conference and Exhibition in Mexico*, September 2006.

[22] V. Baschenko, "Whipstock orientation during drilling of directional wells," *Neft. Gazov. Prom-st.;(Ukrainian SSR)*, vol. 1, 1982.

[23] B. Shu and B. S. Ma, "The return of drilling fluid in large diameter horizontal directional drilling boreholes," *Tunnelling and Underground Space Technology*, vol. 52, pp. 1–11, 2016.

[24] F. Schuh, "Computer makes surge-pressure calculations useful," *Oil and Gas Journal*, vol. 31, p. 96, 1964.

[25] M. E. Baumert and E. N. Allouche, "Methods for estimating pipe pullback loads for horizontal directional drilling (HDD) crossings," *Journal of Infrastructure Systems*, vol. 8, no. 1, pp. 12–19, 2002.

[26] M. E. Baumert, E. N. Allouche, and I. D. Moore, "Experimental investigation of pull loads and borehole pressures during horizontal directional drilling installations," *Canadian Geotechnical Journal*, vol. 41, no. 4, pp. 672–685, 2004.

[27] A. Burman, S. P. Acharya, M. Damodar, and S. Rajeev, "A comparative study of slope stability analysis using traditional limit equilibrium method and finite element method," *Asian Journal of Civil Engineering (Building and Housing)*, vol. 16, 2015.

[28] N. Kumar, A. K. Verma, S. Sardana, K. Sarkar, and T. N. Singh, "Comparative analysis of limit equilibrium and numerical methods for prediction of a landslide," *Bulletin of*

Engineering Geology and the Environment, vol. 77, no. 2, pp. 595–608, 2018.

[29] B. Leshchinsky and S. Ambauen, "Limit equilibrium and limit analysis: comparison of benchmark slope stability problems," *Journal of Geotechnical and Geoenvironmental Engineering*, vol. 141, no. 10, Article ID 04015043, 2015.

[30] Y. Memon, *A Comparison between Limit Equilibrium and Finite Element Methods for Slope Stability Analysis*, Missouri University of Science and Technology, Rolla, MO, USA, 2018.

[31] S. Hazari, R. P. Sharma, and S. Ghosh, "Swedish circle method for pseudo-dynamic analysis of slope considering circular failure mechanism," *Geotechnical & Geological Engineering*, vol. 38, no. 3, pp. 2573–2589, 2020.

[32] T. Zhang, Q. Cai, L. Han, J. Shu, and W. Zhou, "3D stability analysis method of concave slope based on the Bishop method," *International Journal of Mining Science and Technology*, vol. 27, no. 2, pp. 365–370, 2017.

[33] K. Kondo and S. Hayashi, "Similality and generality of the Morgenstern-price and spencer methods," *Landslides*, vol. 34, no. 1, pp. 15–23, 1997.

[34] H. Itasca, *FLAC3D,(Fast Lagrangian Analysis of Continua in 3 Dimensions)*, Itasca Consulting Group, Minneapolis, MN, USA, 2002.

[35] J. Shen and M. Karakus, "Three-dimensional numerical analysis for rock slope stability using shear strength reduction method," *Canadian Geotechnical Journal*, vol. 51, no. 2, pp. 164–172, 2014.